buildings

MDPI

Article

Research on the Influence Mechanism of Moisture Content on Macroscopic Mechanical Response and Microscopic Evolution Characteristic of Limestone

Zhibo Zhang [1,2], Jiang Sun [1], Yankun Ma [2,*], Qi Wang [1], Haotian Li [1] and Enyuan Wang [3]

[1] School of Civil and Resource Engineering, University of Science and Technology Beijing, Beijing 100083, China; zhangzhibo@ustb.edu.cn (Z.Z.); m202320030@xs.ustb.edu.cn (J.S.); 17635240431@163.com (Q.W.); m202320016@xs.ustb.eud.cn (H.L.)
[2] Key Laboratory of Safety and High-Efficiency Coal Mining, Ministry of Education (Anhui University of Science and Technology), Huainan 232001, China
[3] School of Safety Engineering, China University of Mining and Technology, Xuzhou 221116, China; cumtweytop@163.com
* Correspondence: yankunma001@163.com

Abstract: The uniaxial compression experiments and acoustic emission (AE) monitoring are conducted to investigate the macroscopic mechanical behavior and microscopic fracture characteristics of limestone samples with varying moisture contents. The findings revealed that as the moisture content increases from 0 to 6.6%, there is a decrease in peak stress and an increase in peak strain. A clear trend towards greater complexity in fracture characteristics is observed with increasing moisture content. In addition, AE activities demonstrate a heightened frequency, accompanied by an elevation in the corresponding multifractal parameter $\Delta\alpha$ as the moisture content rises. These variations are attributed to the increase in moisture content, which promotes the proliferation of small-scale microcracks and inhibits their evolution into large-scale microcracks. Consequently, the damage and failure process of the limestone samples transitions from being predominantly controlled by a few large-scale microcracks to being collectively influenced by a multitude of small-scale microcracks as the moisture content increases. In conjunction with the Criterion of Microcrack Density, the correctness of the analysis above is substantiated through mathematical derivation. Further, a quantitative model that links the microcrack system to moisture content is established based on the multifractal parameter $\Delta\alpha$. Following this, a characterization model that depicts the macroscopic mechanical properties of limestone affected by moisture content is developed. This model effectively encapsulates the quantitative relationship between moisture content and the macroscopic characteristics of limestone and is validated through fitting experimental data. This research contributes to understanding the macroscopic mechanical response and microscopic fracture characteristics of limestone samples with different moisture contents, providing valuable insights and guidance for ensuring safety during engineering construction processes.

Keywords: moisture content; macroscopic mechanical properties; microscopic evolution characteristic; acoustic emission; microcrack system

Citation: Zhang, Z.; Sun, J.; Ma, Y.; Wang, Q.; Li, H.; Wang, E. Research on the Influence Mechanism of Moisture Content on Macroscopic Mechanical Response and Microscopic Evolution Characteristic of Limestone. *Buildings* **2024**, *14*, 469. https://doi.org/10.3390/buildings14020469

Academic Editor: Eugeniusz Koda

Received: 4 January 2024
Revised: 4 February 2024
Accepted: 6 February 2024
Published: 8 February 2024

1. Introduction

Moisture plays a pivotal role in engineering construction. On the one hand, injecting water into rock effectively prevents rock burst or dust disaster. On the other hand, groundwater seepage into rock fissures can lead to various catastrophes, including collapse, water inrush, and fault slippage. With the increase in the number and scale of engineering construction sites, the risk of water-related dynamic disasters increases significantly, posing significant challenges to the safety and efficiency of engineering construction [1–5]. Therefore, exploring the impact of water on the physical and mechanical properties of rock masses is critical.

Rock, as a natural geological material, exhibits distinct characteristics of discontinuity, heterogeneity, and anisotropy. Factors such as groundwater presence, water injection, hydraulic fracturing, and other natural or anthropogenic influences often result in rock's internal structure having varying water content levels. Studies have shown that changes in water content can affect the physical and mechanical properties of rock masses. Vasarhelyi and Van [6] found that the petrophysical properties of rocks decrease with increasing moisture, and this can result in an increase in mechanical compliance in some cases. Mohamad et al. [7] believed that shale with a higher moisture content exhibits a higher range of anisotropy index. Zhao et al. [8] investigated the acoustic properties of red sandstone under water erosion, and held that the P-wave velocity decreases first and then increases with the increase in moisture content. Zhou et al. [9] observed reductions in sandstone's compressive and tensile strength in different saturation processes under static and dynamic conditions. However, the saturated samples generally regained their mechanical properties and strength in the drying process, akin to their dry state. Chen et al. [10] noted that higher moisture levels facilitated increased slippage in sandstone particles, leading to more plastic deformation and internal energy dissipation. The increase in moisture diminished the brittleness of hard rock, reducing the likelihood of rock bursts. Debanjan et al. [11] observed a general decrease in mechanical properties and fracture toughness in sedimentary rocks with increased saturation. Liu et al. [12] found that the average compressive strength of coal samples decreased by 60.89%, and the failure modes shifted from inclined plane shearing to macrocracking under tensile stress as the saturation pressure rose from 0 to 6 MPa. Liu et al. [13] stated that the variation in water content accelerates the argillization process of mudstone.

Researchers generally agree that changes in the macroscopic physical and mechanical properties of water-bearing rock are closely related to water's impact on the microstructure. Hence, numerous studies have examined the microstructural changes in water-containing rock using advanced testing methods, such as 3D X-ray microanalysis [14], scanning electron microscopy (SEM) [15], nuclear magnetic resonance (NMR) [16], and computed tomography imaging [17]. These methods have been instrumental in exploring the evolving trends in mineral composition, microstructure, and meso structure of rock samples with varying moisture content, shedding light on the microscopic mechanisms of water's influence. Concurrently, various geophysical methods, including ultrasonic technology [18], electromagnetic radiation [19], resistivity [20], and acoustic emission (AE) [21], have been used to analyze the impact of moisture content on the microscopic characteristics of rock masses.

As outlined above, extensive research has been conducted on the physical and mechanical properties, microstructure, fracture, deformation, and failure mechanisms of rock with varying moisture contents, yielding many scientific findings. However, comparative analyses of macroscopic mechanical behavior and microscopic fracture characteristics in rock with differing moisture contents have been scarce, particularly regarding their correlation. In order to bridge this gap, this study analyzes the macroscopic mechanical response of limestone samples with various moisture contents through laboratory experiments. Concurrently, the microscopic fracture characteristics of these limestone samples are investigated using AE monitoring technology. This is followed by a qualitative discussion on the correlation between macroscopic mechanical responses and microscopic fracture characteristics and a more comprehensive quantitative analysis. This research contributes to understanding the macroscopic mechanical response and microscopic fracture characteristics of limestone samples with different moisture contents, providing valuable insights and guidance for ensuring safety during engineering construction processes.

2. Materials and Methods

The limestone sample was sourced from the same piece of limestone, ensuring uniformity by drilling in the same direction to minimize the impact of anisotropy. The limestone

samples were shaped into cylinders (Φ50 × 100 mm) in accordance with the standards set by the International Society for Rock Mechanics through cutting and polishing processes.

To prevent irreversible losses induced by high-temperature drying, all limestone samples were placed in a drying box set at 40 °C for 36 h until the sample weight stabilized. The drying box was then turned off to allow the samples to cool naturally to room temperature, after which their weights were recorded. Subsequently, the dried samples were immersed in deionized water, resulting in four groups of limestone samples with different moisture contents, namely 0 (Dry), 2.7%, 4.3%, and 6.6% (Saturated), whose calculation formula can be expressed as follows:

$$\omega = \frac{m_w - m_d}{m_d} \times 100\% \quad (1)$$

where the parameter ω is the moisture content of the limestone sample; m_w is the weight of the water-containing limestone sample; m_d is the weight of the dry limestone sample.

An electrohydraulic servo press was utilized to conduct uniaxial compression tests on the limestone samples. The loading was carried out in force control mode with a loading rate of 300 N/s. AE signals were collected synchronously throughout this loading process, with a sampling frequency of 1 MHz and a threshold value set at 40 dB. The schematic of the experimental system is depicted in Figure 1.

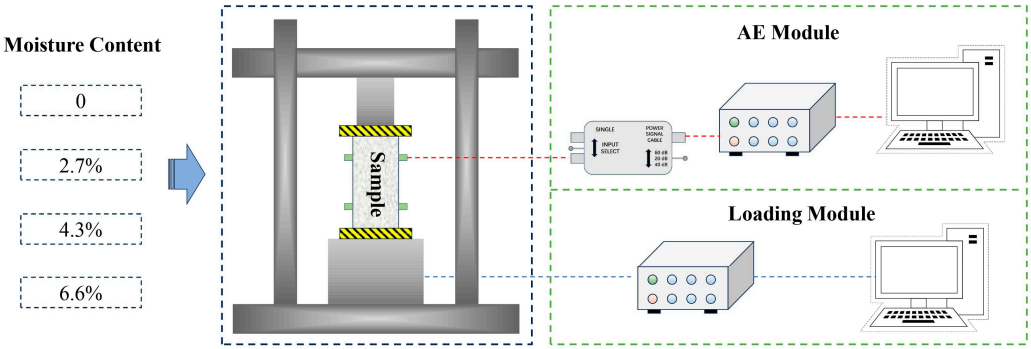

Figure 1. Schematic diagram of experimental system.

3. Experimental Results and Analysis

3.1. Macroscopic Mechanical Characteristics of Limestone Samples

The stress–strain curves for the limestone samples with different moisture contents are displayed in Figure 2a. Figure 2b demonstrates the trends in peak stress and peak strain as a function of moisture content. It is evident that moisture content markedly influenced the limestone samples' macroscopic physical and mechanical characteristics. With increasing moisture content, the peak stress of the limestone samples showed a gradual decline. Compared to the dry limestone samples, the peak stress of limestone samples with moisture contents of 2.7%, 4.3%, and 6.6% diminished by 15.66%, 30.03%, and 49.94%, respectively. In contrast, peak strain incrementally increased with rising moisture content. The peak strain of the limestone samples at moisture contents of 2.7%, 4.3%, and 6.6% was 1.22, 1.26, and 1.63 times greater than that of the dry limestone sample, respectively. Meanwhile, the compaction and post-peak phases also elongated with increasing moisture content, whereas the elastic deformation phase shortened.

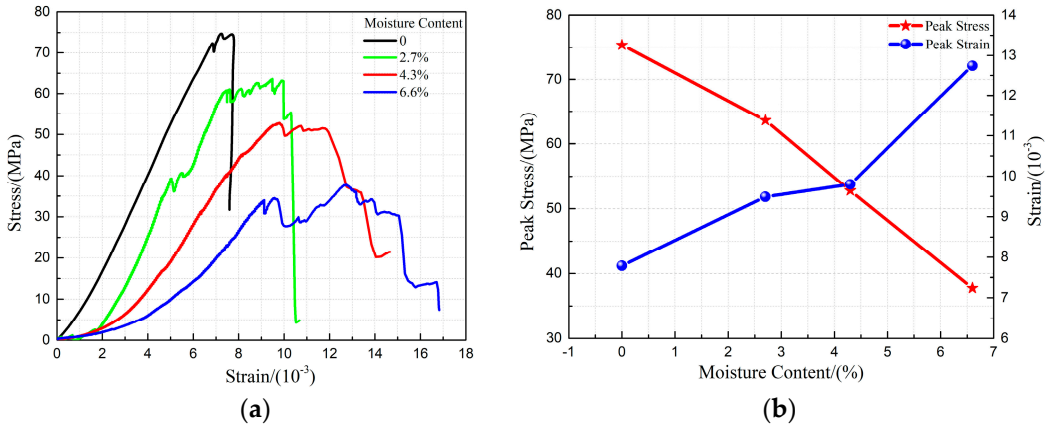

Figure 2. The change in stress and strain with moisture content. (**a**) The stress–strain curves for the limestone samples with different moisture contents, (**b**) The trends in peak stress and peak strain with moisture content.

3.2. Fracture Characteristics of Limestone Samples

The fracture characteristics of the limestone samples signify the ultimate state of microcrack growth and aggregation, providing crucial insights into their mechanical properties and damage processes. Hence, investigating the failure characteristics of limestone samples across varying moisture contents was essential.

Observationally, as the dry limestone sample experienced buckling failure, it fragmented into large blocks with a loud sound, accompanied by a rapid loss of carrying capacity. As moisture content escalated, the intensity of the failure sound decreased, producing numerous fragments. The limestone samples retained some carrying capacity even after exceeding their uniaxial compressive strength.

In this experiment, accurately counting the number of fragments was challenging. Therefore, the weight of the fragments was used for analysis. All fragments were dried before analysis to negate moisture's influence on fragment weight, following the method outlined in Section 2. The limestone sample fragments were then sifted through sieves with varying pore sizes, and the weights of differently sized fragments were measured. As shown in Figure 3, the peak values of the curves progressively shifted leftward with increasing moisture content. As moisture content increased from 0 to 6.6%, the mass proportion of fragments larger than 70 mm plummeted from 82.11% to 0. Conversely, the mass proportion of fragments in the 20–50 mm range rose steadily from 3.82% to 42.61%. This trend indicates a significant increase in smaller fragments as moisture content increases. The mass distribution of fragments evolved from being concentrated in large-scale fragments to dispersed across various fragment sizes.

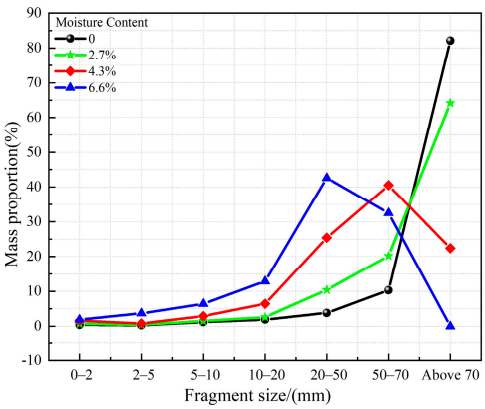

Figure 3. Fragment size distribution characteristics of limestone samples with different moisture contents.

In the macroscopic failure of the limestone sample originated from microcracks, the formation of microcracks was linked to smaller-scale microcracks. This self-similar behavior resulted in the fragments exhibiting self-similar characteristics. According to fractal theory and the box-counting method [22–25], the fractal characteristics of the discrete fragments were calculated using Equation (2).

$$N = Cr^{-D} \tag{2}$$

where N is the number of discrete fragments whose size exceeds r; C is a material constant; D is the fractal dimension of discrete fragments.

Taking the logarithm of both sides of Equation (2), Equation (3) can be obtained as follows:

$$\log N = \log C - D \log r \tag{3}$$

The fractal dimension was represented by the slope of the fitted line in the log(r)-log(N) coordinate system, and the calculation results indicated that fractal dimension increases from 2.38 to 2.93 with rising moisture content. This suggested that an increase in moisture content results in a more intricate size distribution of fragments, transforming the fracture mode from simple to complex. By using the data fitting method, the relationship between the fractal dimension of fragments and moisture content can be expressed by a linear function with a fitting coefficient of 0.9997, as shown in Figure 4.

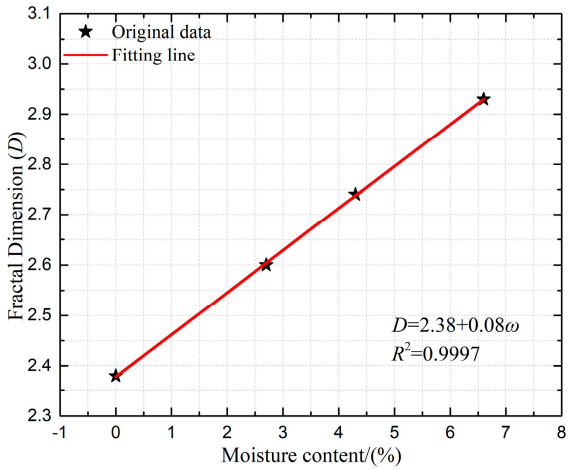

Figure 4. Fractal dimension and fitting line of fragment size distribution of limestone samples with different moisture contents.

4. AE Characteristics of Limestone Samples

4.1. AE Energy Evolution Characteristics

In order to explore the microscopic perspective of the damage evolution process in limestone samples with varying moisture contents, AE activities generated by the cracking of limestone samples were continuously collected throughout the experiment. The evolution characteristics of AE energy are depicted in Figure 5. The AE signal became more abundant with increasing moisture content, yet the AE cumulative energy decreased. As moisture content increased from 0 to 6.6%, the maximum AE energies were 63,321, 10,622, 5744, and 2105 mv*μs, respectively, while the AE cumulative energies were 515,032, 418,094, 305,234, and 192,408 mv*μs, respectively. The maximum AE energy and AE cumulative energy of the dry limestone sample were 30.12 and 2.74 times that of the saturated limestone sample, respectively.

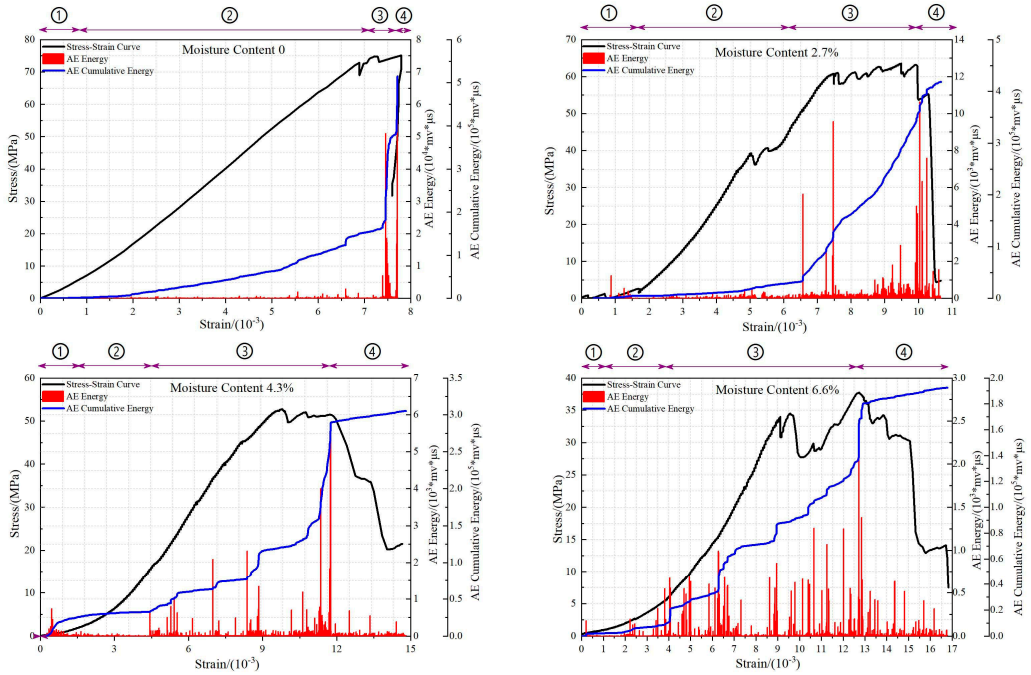

Figure 5. AE energy evolution characteristics of limestone samples with different moisture contents.

Figure 5 indicates that the evolution characteristics of AE energy can be divided into four stages: initial-active stage (represented by ① in Figure 5), calm stage (represented by ② in Figure 5), increasing stage (represented by ③ in Figure 5), and post-peak stage (represented by ④ in Figure 5).

(1) Initial-active stage: At this stage, preexisting microcracks gradually closed as loading commenced. The relative dislocation and mutual friction of particles led to the release of partial energy in elastic waves, initiating AE signal generation.

(2) Calm stage: As stress increased, preexisting microcracks closed completely, but new microcracks had not yet formed. AE signals primarily resulted from the dislocation of closed microcrack surfaces and grain deformation, leading to a small number of AE activities.

(3) Increasing stage: With continuing stress increase, stress concentration occurred at microcrack tips, generating new microcracks. Before the buckling failure of the limestone samples, elevated stress accelerated microcrack growth. The generation and interaction of numerous microcracks caused a rapid rise in AE activities.

(4) Post-peak stage: The limestone sample had experienced macroscopic failure in this stage, and its strength had significantly diminished. As the load decreased rapidly, the AE activity also declined rapidly.

The AE energy evolution process exhibited common characteristics across limestone samples with different moisture contents, yet notable differences were observed. In the initial-active stage, AE activities in water-containing limestone samples surpassed those in dry samples. However, the calm stage in water-containing limestone samples was comparatively briefer and less distinct than in dry samples. With increasing moisture content, the increasing and post-peak stages extended, accompanied by a surge in AE activities.

4.2. Multifractal Characteristics of AE Energy

To further analyze quantitatively the differences in AE energy characteristics of limestone samples with varying moisture contents, the box-counting method was used to calculate the multifractal spectrum of the AE energy series [26,27], as shown in Equations (4)–(6).

$$X_q(\varepsilon) \equiv \sum P_i(\varepsilon)^q \sim \varepsilon^{\tau(q)} \quad (4)$$

$$\alpha = \frac{d(t(q))}{dq} = \frac{d}{dq}\left(\lim_{\varepsilon \to 0} \frac{\ln X_q(\varepsilon)}{\ln \varepsilon}\right) \tag{5}$$

$$f(\alpha) = \alpha q - \tau(q) \tag{6}$$

where α is a constant known as the singularity exponent; $f(\alpha)$ is the frequency of the subset represented by α in the whole subsets. The curve composed of α and $f(\alpha)$ represents the multifractal spectrum of the research series, reflecting the uneven distribution of the AE energy series. Defining $\Delta\alpha = \alpha_{max} - \alpha_{min}$, the parameter $\Delta\alpha$ represents the uneven distribution of the AE energy, reflecting the irregularity and complexity of the microfracture scale.

The multifractal spectrums of the AE energy series of limestone samples with different moisture contents were calculated, and the changing trend in multifractal parameter $\Delta\alpha$ was analyzed, as shown in Figure 6. The multifractal spectrum was narrow when the moisture content was low, indicating that the AE energy distribution was relatively simple. The multifractal spectrum gradually widened with increased moisture content, indicating that the AE energy distribution became more irregular. Therefore, it can be inferred that the damage and failure processes of the limestone samples became more complex with increasing moisture content. Based on the analysis results, data fitting shows that the multifractal parameter $\Delta\alpha$ had a linear relationship with moisture content, with a fitting coefficient of 0.9725.

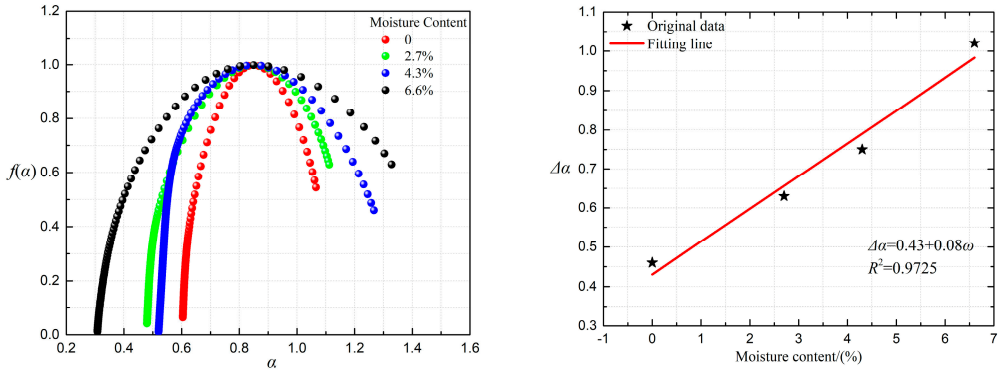

Figure 6. Multifractal characteristics of AE energy of limestone samples with different moisture contents. (**a**) Multifractal spectrum; (**b**) Change in multifractal parameter $\Delta\alpha$ and corresponding fitting line.

5. Discussion

5.1. Qualitative Analysis

Limestone contains numerous highly hydrophilic mineral particles. When water infiltrates limestone through microcracks, free water molecules create a film around these particles, smoothing their irregular, jagged edges. This process reduces friction among the mineral particles, facilitating the growth of microcracks. Concurrently, both physically and chemically, water interacts with the organic and inorganic matter in limestone, weakening its internal cemented structure. Primary microcracks enlarge, and primary holes expand gradually, increasing the degree of freedom for microcrack growth. This leads to the full development of microcracks at lower stress levels. Furthermore, water is thought to maintain a dynamic equilibrium within the pore structure of limestone. External loading may cause water in the pores to generate pressure, encouraging further development of the microcrack system.

Aligning with the Criterion of Microcrack Density [28,29], large-scale microcracks are formed by the interaction of small-scale microcracks. Hence, during the loading process of dry limestone samples, small-scale microcracks, A_1, require external energy to grow into larger-scale microcracks, A_2, culminating in the largest-scale cracks, A_n, before the

sample's buckling failure. When the limestone sample contains moisture, the small-scale microcracks, B_1, need comparatively less energy to grow and form larger-scale microcracks, B_2, due to moisture's enhancing effect on microcrack development. Before buckling failure, the largest-scale cracks, B_m, form in the moist limestone sample.

The experimental and analytical findings suggest that the scale of microcracks, A_1, can be comparable to that of microcracks, B_1. However, the scales of microcracks, B_2 and B_m, are smaller than those of microcracks, A_2 and A_n. Additionally, the transformation frequency parameter m exceeds the parameter n. This observation implies that an increase in moisture content accelerates the transformation of microcracks but limits their maximum scale. Consequently, as moisture content rises, AE activities become more frequent and complex, while activities with higher energy levels decrease.

Limestone is conceptualized, by employing the effective medium theory, as a complex system comprising the matrix and microcrack systems, which significantly influence its macroscopic mechanical properties together. The matrix system mainly consists of various mineral particles, whereas the microcrack system represents the voids created by microfractures. Generally, the matrix system remains relatively stable under external loads, and changes in the microcrack system primarily drive alterations in limestone's macroscopic mechanical properties. Continuous development of the microcrack system enhances its impact on limestone samples, manifesting properties associated with the microcrack system. Conversely, the gradual reduction of the microcrack system diminishes its influence, leading to more pronounced characteristics of the matrix system [30]. Building on this analysis, it is clear that higher moisture content increases the complexity of microcracks, causing limestone samples to exhibit more distinct features of the microcrack system. As a result, the peak stress decreases, peak strain increases, and the failure characteristics of the limestone samples become more complex with increased moisture content.

5.2. Quantitative Analysis

The previous analysis shows damage and failure progression in the limestone sample as a sequential transformation from small-scale to larger-scale microcracks, and this transformation adheres to the function described by Equation (7).

$$K = \frac{R}{L} \tag{7}$$

where L is the scale of microcracks; R is the distance between these microcracks; K is the crack aggregation density criterion, illustrating the microcracks' interaction capability.

Equation (7) indicates that a higher value of parameter K signifies a reduced interaction capability among microcracks. Reaching the critical stress threshold leads to the formation of high-energy and large-scale microcracks. Thus, parameter K indirectly reflects the energy released and the scale of the microfractures. A higher value of K corresponds to greater released energy and a larger microfracture scale.

Further, Zhurkov et al. [31,32] introduced a novel function to illustrate this process, as shown in Equation (8).

$$P_m \propto \left[\frac{e}{K}\right]^m \tag{8}$$

where P_m is the probability of interaction occurrence among m microcracks; e is the base of the natural logarithm.

Based on the above analysis, Equation (9) can be derived by generalizing Equation (8),

$$N(K) \propto \left[\frac{E}{K}\right]^M \tag{9}$$

where $N(K)$ is the number of different-scale microcracks; M is the complexity degree of the microcrack system; E correlates with the physical and mechanical characteristics of

limestone samples, where more complete limestone samples correspond to higher values of parameter E.

Based on Equation (9), it is evident that parameter M governs the shape of the function curve, while parameter E influences its position. As moisture promotes microcrack development, increasing moisture content leads to a reduction in parameter E and an elevation in parameter M. As depicted in Figure 7, a marked decrease in the corresponding microcrack number is observable with the escalation of the microcrack scale in limestone samples with varying moisture contents. This phenomenon intensifies with higher moisture content. The points where curves of dry limestone samples intersect with those at moisture levels of 2.7%, 4.3%, and 6.6% are designated as A, B, and C, respectively. These intersection points progressively shift upward and leftward from A to C. This suggests that escalating moisture content encourages the proliferation of small-scale microcracks while restraining the transition to large-scale microcracks, corroborating the earlier analysis in Section 5.1 from a theoretical perspective.

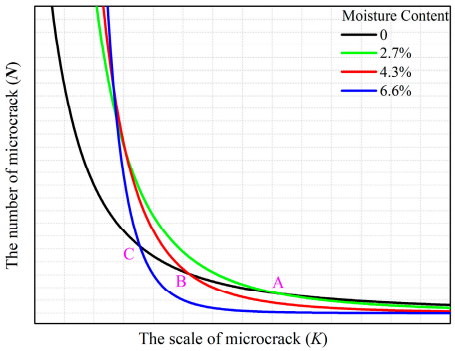

Figure 7. Schematic diagram of correlation between microcrack scale and microcrack number of limestone samples with different moisture contents.

In this study, the multifractal parameter $\Delta\alpha$ of AE energy functions as an indicator of microcrack complexity, reflecting the physical and mechanical properties of the limestone samples. Hence, Equation (9) can be modified to Equation (10).

$$N(K) \propto \left[\frac{T}{K}\right]^{\Delta\alpha} \tag{10}$$

where parameter T is related to parameters E and $\Delta\alpha$.

The volume V of the microcrack system can be expressed as,

$$V_c = K^{\Delta\alpha} N(K) \sim T^{\Delta\alpha} \tag{11}$$

Incorporating effective medium theory and the quantitative relationship between moisture content ω, and multifractal parameter $\Delta\alpha$, the limestone samples' peak strength and peak strain are described by Equation (12).

$$\begin{aligned} \sigma &= -\eta_1 V_c + \varphi_1 = -\eta_1 T^{(0.08\omega+0.43)} + \varphi_1 \\ \varepsilon &= \eta_2 V_c + \varphi_2 = \eta_2 T^{(0.08\omega+0.43)} + \varphi_2 \end{aligned} \tag{12}$$

where, the parameters σ and ε represent the peak stress and peak strain, respectively. The parameters η and φ are the correlation coefficient, which can be obtained by data fitting.

Figure 8 demonstrates that Equation (12) effectively captures the evolution process of peak strength and peak strain in limestone samples with diverse moisture contents. The high fitting coefficient underscores the model's robustness in depicting this relationship.

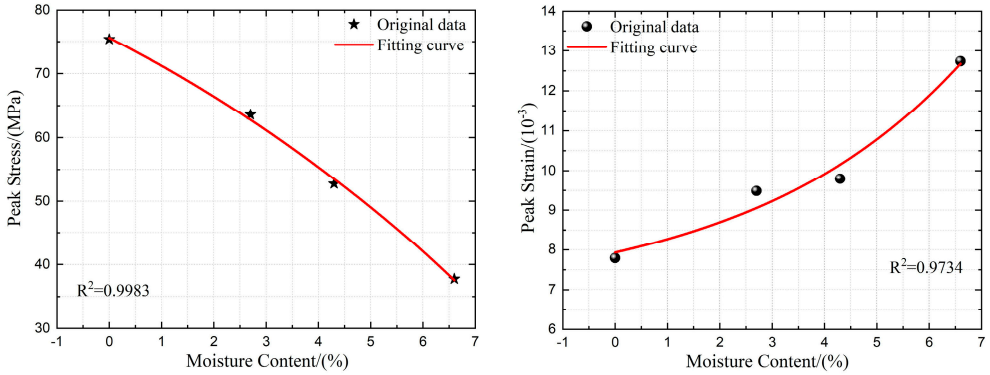

Figure 8. Experimental data and fitting relationship of macroscopic mechanical characteristics of limestone samples with different moisture contents.

Accordingly, increasing moisture content promotes the proliferation of small-scale microcracks and impedes their growth into large-scale microcracks. Moisture alters the macroscopic characteristics of limestone samples by affecting the microcrack system, revealing a pronounced nonlinear interrelation.

6. Conclusions

This study presents uniaxial compression experiments to analyze the macroscopic mechanical properties of limestone samples with varied moisture contents. It also utilizes AE monitoring technology to investigate the corresponding microscopic damage evolution characteristics. The study meticulously examines the influence of moisture content on both the macroscopic and microscopic mechanical traits of limestone samples, elucidating their quantitative relationship. The primary research findings include:

(1) With moisture content rising from 0 to 6.6%, a gradual decrease in peak stress and an increase in peak strain in the limestone samples are noted. The compaction and post-peak phases extend while the elastic deformation phase shortens. Concurrently, a decrease in failure loudness and an increase in the number of fragments occur. The fractal dimension of fragment distribution increases from 2.38 to 2.93, signifying a shift in macroscopic fracture mode from simple to complex with rising moisture content.

(2) Enhanced moisture content leads to more prevalent AE activities, while cumulative AE energy decreases. Compared to dry limestone samples, those containing water exhibit shorter, less distinct calm stages but more pronounced increasing and post-peak stages. Additionally, the multifractal spectra of the AE energy series show narrower profiles at lower moisture contents, indicating a simpler AE energy distribution. In contrast, higher moisture content widens the multifractal spectrum, suggesting an irregular distribution of AE energy. It can be inferred that a higher moisture content facilitates and complicates the development of the microcrack system.

(3) An increase in moisture content encourages the proliferation of small-scale microcracks while inhibiting their enlargement into larger-scale microcracks. This change manifests as a transformation in the damage and failure process of limestone samples, transitioning from domination by a few large-scale microcracks to collective influence by numerous small-scale microcracks as the moisture content rises. Consequently, increasing moisture content makes AE activities more abundant and intricate, but higher-energy-level activities diminish. From a macroscopic perspective, an increase in moisture content results in expressing more properties of the microcrack system, presenting decrease in peak stress and increase in peak strain.

(4) The assertion that increasing moisture content promotes the proliferation of small-scale microcracks while hindering their transition to large-scale microcracks is substantiated through mathematical derivation. A characterization model is developed to describe the macroscopic mechanical properties of the limestone sample influenced by moisture content. This model effectively captures the quantitative relationship be-

tween moisture content and the macroscopic characteristics of limestone, corroborated by experimental data fitting.

This research contributes to understanding the macroscopic mechanical response and microscopic fracture characteristics of limestone samples with different moisture contents, providing valuable insights and guidance for ensuring safety during engineering construction processes.

Author Contributions: Conceptualization, Z.Z. and Y.M.; methodology, Z.Z., J.S. and E.W.; software, Y.M. and Q.W.; validation, Z.Z., E.W. and Y.M.; formal analysis, Z.Z. and J.S.; investigation, Z.Z. and H.L.; resources, Z.Z.; data curation, Z.Z., J.S. and Q.W.; writing—original draft preparation, Z.Z. and J.S.; writing—review and editing, Z.Z., J.S. and Y.M.; visualization, Z.Z. and Q.W.; supervision, Z.Z.; project administration, Z.Z.; funding acquisition, Z.Z. All authors have read and agreed to the published version of the manuscript.

Funding: This research was funded by "the Research Funds for Key Laboratory of Safe and High-Effective Coal Mining, Ministry of Education (Anhui University of Science and Technology) (JYB-SYS2021207)", and "The Research Fund of The State Key Laboratory of Coal Resources and Safe Mining, CUMT (SKLCRSM21KF009)".

Data Availability Statement: The raw data supporting the conclusions of this article will be made available by the authors on request.

Conflicts of Interest: The authors declare no conflicts of interest.

References

1. Sakhno, I.; Sakhno, S. Numerical studies of floor heave mechanism and the effectiveness of grouting reinforcement of roadway in soft rock containing the mine water. *Int. J. Rock Mech. Min. Sci.* **2023**, *170*, 105484. [CrossRef]
2. Vásárhelyi, B.; Davarpanah, M. Influence of water content on the mechanical parameters of the intact rock and rock mass. *Period. Polytech. Civ. Eng.* **2018**, *62*, 1060–1066. [CrossRef]
3. Shen, R.; Li, H.; Wang, E.; Chen, T.; Li, T.; Tian, H.; Hou, Z. Infrared radiation characteristics and fracture precursor information extraction of loaded sandstone samples with varying moisture contents. *Int. J. Rock Mech. Min. Sci.* **2020**, *130*, 104344. [CrossRef]
4. Li, N.; Huang, B.; Zhang, X.; Tan, Y.; Li, B. Characteristics of microseismic waveforms induced by hydraulic fracturing in coal seam for coal rock dynamic disasters prevention. *Saf. Sci.* **2019**, *115*, 188–198. [CrossRef]
5. Zhou, Z.; Cai, X.; Ma, D.; Cao, W.; Chen, L.; Zhou, J. Effects of water content on fracture and mechanical behavior of sandstone with a low clay mineral content. *Eng. Fract. Mech.* **2018**, *193*, 47–65. [CrossRef]
6. Vasarhelyi, B.; Ván, P. Influence of water content on the strength of rock. *Eng. Geol.* **2006**, *84*, 70–74. [CrossRef]
7. Mohamad, E.T.; Aziz, A.A.; Maiye, O.M.; Liang, M. The effect of moisture content on the strength and anisotropy index of tropically weathered shale. *Electron. J. Geotech. Eng.* **2013**, *18*, 5967–5979.
8. Zhao, K.; Ran, S.; Zeng, P.; Yang, D.X.; Teng, T.Y. Effect of moisture content on characteristic stress and acoustic emission characteristics of red sandstone. *Rock Soil Mech.* **2021**, *42*, 2.
9. Zhou, Z.; Cai, X.; Cao, W.; Li, X.; Xiong, C. Influence of water content on mechanical properties of rock in both saturation and drying processes. *Rock Mech. Rock Eng.* **2016**, *49*, 3009–3025. [CrossRef]
10. Chen, G.; Li, T.; Guo, F.; Wang, Y. Brittle mechanical characteristics of hard rock exposed to moisture. *Bull. Eng. Geol. Environ.* **2017**, *76*, 219–230. [CrossRef]
11. Guha Roy, D.; Singh, T.N.; Kodikara, J.; Das, R. Effect of water saturation on the fracture and mechanical properties of sedimentary rocks. *Rock Mech. Rock Eng.* **2017**, *50*, 2585–2600. [CrossRef]
12. Liu, X.; Long, K.; Luo, P.; Luo, Y. Effects of Water Saturation Pressure on Crack Propagation in Coal under Uniaxial Compression. *Nat. Resour. Res.* **2023**, *32*, 673–690. [CrossRef]
13. Liu, B.; Yang, H.; Karekal, S. Effect of water content on argillization of mudstone during the tunnelling process. *Rock Mech. Rock Eng.* **2020**, *53*, 799–813. [CrossRef]
14. Yao, Q.; Chen, T.; Tang, C.; Sedighi, M.; Wang, S.; Huang, Q. Influence of moisture on crack propagation in coal and its failure modes. *Eng. Geol.* **2019**, *258*, 105156. [CrossRef]
15. Yang, X.; Wang, J.; Zhu, C.; He, M.; Gao, Y. Effect of wetting and drying cycles on microstructure of rock based on SEM. *Environ. Earth Sci.* **2019**, *78*, 1–10. [CrossRef]
16. Yang, K.; Connolly, P.R.J.; Li, M.; Seltzer, S.J.; McCarty, D.K.; Mahmoud, M.; Johns, M.L. Shale rock core analysis using NMR: Effect of bitumen and water content. *J. Pet. Sci. Eng.* **2020**, *195*, 107847. [CrossRef]
17. Jiang, L.; Xu, Y.; Chen, B.; Wu, B. Effect of water content on the mechanical properties of an artificial porous rock. *Bull. Eng. Geol. Environ.* **2021**, *80*, 7669–7681. [CrossRef]

18. Duan, T.; Ren, Y. Study on uniaxial compression mechanical properties of sandstone with different moisture content and wave velocity method. *Coal Geol. Explor.* **2019**, *47*, 24.
19. Li, H.; Qiao, Y.; Shen, R.; He, M. Electromagnetic radiation signal monitoring and multi-fractal analysis during uniaxial compression of water-bearing sandstone. *Measurement* **2022**, *196*, 111245. [CrossRef]
20. Jin, Y.; Zhang, T.; Hua, Z.; Xu, M.; Huang, P. The electrical resistivity changes and volumetric strain of water-bearing cracked rock samples under uniaxial compression. *Acta Seismol. Sin.* **2011**, *5*, 99–106.
21. Zhu, J.; Deng, J.; Chen, F.; Wang, F. Failure analysis of water-bearing rock under direct tension using acoustic emission. *Eng. Geol.* **2022**, *299*, 106541. [CrossRef]
22. Yao, Q.; Wang, W.; Zhu, L.; Xia, Z.; Tang, C.; Wang, X. Effects of moisture conditions on mechanical properties and AE and IR characteristics in coal–rock combinations. *Arab. J. Geosci.* **2020**, *13*, 1–15. [CrossRef]
23. Zhang, Z.; Wang, E.; Li, N. Fractal characteristics of acoustic emission events based on single-link cluster method during uniaxial loading of rock. *Chaos Solitons Fractals* **2017**, *104*, 298–306. [CrossRef]
24. Xue, K.; Zhang, Z.; Han, X.; Guang, W. A fractal model for estimating the permeability of tortuous fracture networks with correlated fracture length and aperture. *Phys. Fluids* **2023**, *35*, 043615.
25. Panigrahy, C.; Seal, A.; Mahato, N.K.; Bhattacharjee, D. Differential box counting methods for estimating fractal dimension of gray-scale images: A. survey. *Chaos Solitons Fractals* **2019**, *126*, 178–202. [CrossRef]
26. Aouit, D.A.; Ouahabi, A. Nonlinear fracture signal analysis using multifractal approach combined with wavelets. *Fractals* **2011**, *19*, 175–183. [CrossRef]
27. Zhang, Z.; Wang, E.; Zhang, H.; Bai, Z.; Zhang, Y.; Chen, X. Research on nonlinear variation of elastic wave velocity dispersion characteristic in limestone dynamic fracture process. *Fractals* **2023**, *31*, 2350008. [CrossRef]
28. Zhurkov, S.N.; Kuksenko, V.S.; Petrov, V.A. Principles of the kinetic approach of fracture prediction. *Theor. Appl. Fract. Mech.* **1984**, *1*, 271–274. [CrossRef]
29. Zhang, Z.; Liu, X.; Zhang, Y.; Qin, X.; Khan, M. Comparative study on fracture characteristics of coal and rock samples based on acoustic emission technology. *Theor. Appl. Fract. Mech.* **2021**, *111*, 102851. [CrossRef]
30. Zhang, Z.; Wang, E.; Li, N.; Zhang, H.; Bai, Z.; Zhang, Y. Research on macroscopic mechanical properties and microscopic evolution characteristic of sandstone in thermal environment. *Constr. Build. Mater.* **2023**, *366*, 130152. [CrossRef]
31. Zavyalov, A.D. From the kinetic theory of strength and fracture concentration criterion to the seismogenic fracture density and earthquake forecasting. *Phys. Solid State* **2005**, *47*, 1034–1041. [CrossRef]
32. Zavyalov, A.D. Medium-term prediction of earthquakes from a set of criteria: Principles, methods, and implementation. *Russ. J. Earth Sci.* **2005**, *7*, 51–73. [CrossRef]